

Review

Thin Film Thermoelectric Materials: Classification, Characterization, and Potential for Wearable Applications

Xinqi Chen ^{1,2}, Wei Dai ¹, Tian Wu ¹, Wei Luo ^{2,*}, Jianping Yang ² , Wan Jiang ^{2,3} and Lianjun Wang ^{2,*}

¹ School of Physics and Mechanical & Electrical Engineering, Hubei University of Education, Wuhan 430205, China; chenxinqi@hue.edu.cn (X.C.); daiwei@hue.edu.cn (W.D.); twu@whu.edu.cn (T.W.)

² State Key Laboratory for Modification of Chemical Fibers and Polymer Materials, College of Materials Science and Engineering, Donghua University, Shanghai 201620, China; jianpingyang@dhu.edu.cn (J.Y.); wanjiang@dhu.edu.cn (W.J.)

³ School of Materials Science and Engineering, Jingdezhen Ceramic Institute, Jingdezhen 333001, China

* Correspondence: wluo@dhu.edu.cn (W.L.); wanglj@dhu.edu.cn (L.W.); Tel.: +86-21-6787-4091 (W.L.)

Received: 22 May 2018; Accepted: 9 July 2018; Published: 10 July 2018



Abstract: Thermoelectric technology has the ability to convert heat directly into electricity and vice versa. With the rapid growth of portable and wearable electronics and miniature devices, the self-powered and maintenance of free thermoelectric energy harvester is highly desired as a potential power supply. Thin film thermoelectric materials are lightweight, mechanically flexible, and they can be synthesized from abundant resources and processed with a low-cost procedure, which offers the potential to develop the novel thermoelectric devices and hold unique promise for future electronics and miniature accessories. Here, a general classification for thin film thermoelectric materials varied by material compositions, and thermoelectric properties depended on different measurement technique. Several new flexible thermoelectric strategies are summarized with the hope that they can inspire further development of novel thermoelectric applications.

Keywords: thermoelectric materials; thin film; organic materials; composite materials; energy conversion; thermoelectric devices

1. Introduction

Thermoelectric (TE) technology, converting heat into electricity directly and vice versa, is significant facing recent energy crisis [1–7]. When the heat flow passes through the TE device, the temperature difference between the hot end and the cold end generates the current, and the motion of the current makes the device heat or cool. This practical application attracts a lot of research interests, however, TE conversion technology is not for typical use in daily life due to the low conversion efficiency. The efficiency of TE device, as determined by electrons passing from *p*-type materials to *n*-type materials, can be improved via optimizing the property of TE materials [8]. The efficiency of TE materials is expressed by the dimensionless TE figure of merit (*ZT*). $ZT = S^2\sigma T/\kappa$, where *S* is the Seebeck coefficient, σ is the electrical conductivity, κ is the thermal conductivity, and *T* is the absolute temperature [9,10]. The higher *ZT* value demonstrated, the better TE performance of the semiconductor materials [11–13].

Conventional bulk TE materials have a long research history, dating back to Seebeck discovered the phenomenon of “thermomagnetism” in 1821 [14–16]. These materials are mainly based on elements, like Bi, Te, Sb, Pb, etc., including typical inorganic materials of Bi₂Te₃, PbTe, SiGe, skutterudite, and half-Heusler alloys [17–19]. To this date, the highest reported *ZT* value is still below 3, which limits

the usage of thermoelectric energy conversion to niche applications. Reaching higher ZT value can realize the efficient conversion for widespread commercial TE device applications [20–24]. Furthermore, bulk TE materials encountered a bottleneck in practical application, such as limitation of shape and stagnancy of performance, which restricted the development of intelligent TE devices. In contrast, thin film TE materials are lightweight and low cost and are easily synthesized on different kinds of substrates, which offer possibility in the development of novel TE devices meeting bendable and miniature requirements [25–28].

In this review, we discuss the general classification, typical synthesis approaches, and TE measurement technique of thin film TE materials. Three kinds of thin film TE materials, inorganic based, organic based, and inorganic-organic composite thin film TE materials, are introduced with their common synthetic methods. Some novel TE measurement technique for electrical conductivity, Seebeck coefficient, and thermal conductivity of thin film TE materials are mentioned. Finally, several new perspectives for the further development of novel TE devices are outlined.

2. Classification of Thin-Film TE Materials

2.1. Inorganic-Based Thin Film TE Materials

Inorganic bulk TE materials are limited in their application by their low efficiency and high cost. It has been shown recently that the low-dimensional material design improves TE efficiency through more effective phonon scattering, thus contributing strongly to a reduced lattice thermal conductivity [29]. Some theories explain that quantum well effect and superlattice structure of thin films determine these better TE properties [18]. The following section is the fabricated thin films of typical inorganic TE materials system and their TE performance.

2.1.1. Bi-Te Based Superlattices

In the last two decades, Bi-Te based bulk materials have improved their TE performance by doping. When compared with single-phase Bi_2Te_3 , the samples dispersed with Ag nanoparticles exhibited the much lower thermal conductivity and higher power factor. A maximum ZT value of 0.77 obtained at 475 K from the bulk Bi_2Te_3 dispersed with 2.0 vol % Ag nanoparticles, approximately three times higher than that of the pristine bulk Bi_2Te_3 [30]. Similarly, Bi-Te based superlattices have been studied with doping and their ZT values were measured in thin film TE devices, which showed a great performance (Figure 1a) [31,32]. For example, low-temperature growth process in metal-organic chemical vapor deposition has been used for Bi_2Te_3 system thin film for preparation of the individual layer as small as 10 Å [31,33]. In this work, *p*-type $\text{Bi}_2\text{Te}_3/\text{Sb}_2\text{Te}_3$ superlattices and *n*-type $\text{Bi}_2\text{Te}_3/\text{Bi}_2\text{Te}_{2.83}\text{Se}_{0.17}$ superlattices thin films showed ZT value ~2.4 and ~1.4 at 300 K, separately. Besides, regarding the reduction of production cost of this material system, *p*-type $\text{Bi}_{0.4}\text{Te}_{3.0}\text{Sb}_{1.6}$ and *n*-type $\text{Bi}_{2.0}\text{Te}_{2.7}\text{Se}_{0.3}$ thin films were fabricated by a flash evaporation method (Figure 1b,c) [32]. This deposition method depends on a simple equipment that has three parts, including a vacuum chamber with particle holder, tungsten heater, and a substrate holder. The *p*-type and *n*-type spherical powders of TE thin films with average size 200 μm on glass substrates result in the good electrical performance, which reach $15.9 \mu\text{W cm}^{-1} \text{K}^{-2}$ in power factor of *p*-type thin film and $21.5 \mu\text{W cm}^{-1} \text{K}^{-2}$ in power factor of the *n*-type thin film. However, when comparing to the Bi-Te system thin film TE devices, less cost Zn based thin films and Cu based thin films have been studied recently [27,28,34,35].

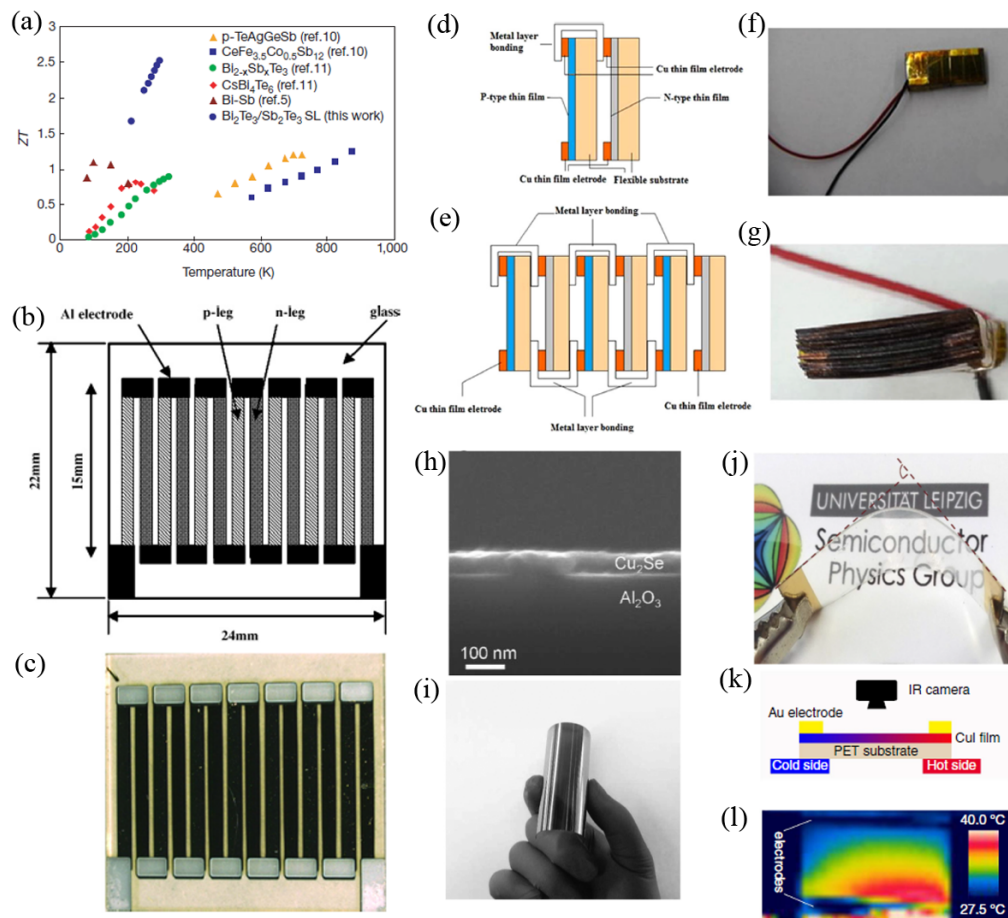


Figure 1. (a) Temperature dependence of figure of merit (ZT) of 10 Å/50 Å *p*-type Bi₂Te₃/Sb₂Te₃ superlattice compared to those of several recently reported materials. Reproduced from [31] with permission; Copyright Nature Publishing Group 2001; Schematic illustration (b) and photograph (c) of the bismuth-telluride-based alloy thin film thermoelectric (TE) generator. Reproduced [32] with permission; Copyright Elsevier 2007; Schematic illustration of the Zn based thin film TE generator (TFTEG): (d) A *p*-*n* couple was formed through connecting the *n*-type Al-doped ZnO and *p*-type Zn-Sb based thin films by metal layer bonding with Cu films deposited on both sides of the substrate; (e) Structure of the whole TFTEG; (f) and (g) are pictures of real Zn based TFTEG products. Reproduced [35] with permission; Copyright AIP Publishing 2015; (h) Cross-section scanning electron microscopic (SEM) image of the Cu₂Se thin film on Al₂O₃ substrate; (i) Photograph of the Cu₂Se thin film on the polyimide substrate. Reproduced [27] with permission; Copyright John Wiley & Sons, Inc. 2017; (j) The photograph of a CuI thin film sample deposited on polyethylene terephthalate (PET) substrate with a bending angle; (k) Schematic illustration for the power output measurement of the CuI/PET single-leg TE device; and, (l) The example infrared image taken during one of the measurements. Reproduced from [28] with permission; Copyright Nature Publishing Group 2017.

2.1.2. Zn Based Thin Films

ZnO thin film has numerous applications in an energy-related area, including various metal-doped ZnO thin film in TE application [36,37]. Among them, Al-doped ZnO thin film can serve as high-temperature TE modules for practical applications. At the preparation step, the direct current (DC) magnetic sputtering method was selected in the deposition of the metal-based film due to its high purity, large-scale, and low cost. Based on this method, *n*-type Al-doped ZnO thin film that was deposited on glass substrates at room temperature. After measurement, the ZnO with 3 wt % Al-doped thin film reaches the maximum power factor of 1.54 μW/cm K² [34]. The maximum power

output of Al-doped ZnO film is 2.3 nW for a temperature gradient of 20 K near room temperature, which is more practical for TE devices [38]. Beyond the hard substrates, *n*-type Al-doped ZnO and *p*-type Zn-Sb based thin film were deposited on the flexible substrate with the thickness of 0.15 mm. The final assembled TE devices with ten couples showed maximum output power 246.3 μ W in a 180 K temperature difference (Figure 1d–g) [35].

2.1.3. Cu Based Thin Films

Copper-based composites, no matter in bulk form or thin film, have attracted much attention in TE application [21,22,39–41]. The Cu₂Se bulk has been reported reaching the highest ZT value of 2.4 at 1000 K [42]. The excellent TE performance of copper selenide crystals is related to their lower lattice thermal conductivity [21,22]. Nevertheless, the research on Cu₂Se thin films exhibits lower TE performance than that in bulk form. A method for thin flexible films deposition using high-performance Cu₂Se powders has found recently. In this approach, the Cu₂Se powder was dissolved in the organic solution making an ink solution. Then, through the wet-deposition method, this ink solution was covered on flexible substrates evenly (Figure 1h,i). The Cu₂Se thin film fabricated by this route exhibits a power factor of 0.62 mW cm⁻¹ K⁻² at 684 K [27]. Furthermore, the TE generators working in room temperature range will be a significant breakthrough in the development of wearable and portable devices. CuI in its γ -phase or low temperature is a *p*-type conductor [28]. Recent research explored that γ -CuI thin film has a large Seebeck coefficient and hole conductivity, as well as low thermal conductivity. These polycrystalline CuI thin films were deposited on glass by reactive sputtering at room temperature (Figure 1j). A high purity copper target was used for sputtering and iodine vapor was injected by a needle valve from gasified iodine source. The measured hole conduction of these *p*-type undoped CuI thin film is 156 S/cm and I-doped CuI thin film is 283 S/cm (Figure 1k,l) [43]. The total figure of merit ZT of CuI thin film is 0.21 at 300 K. These CuI thin films, the thickness of 200–300 nm, were able to assemble as transparent and flexible TE modules opening a path for future flexible TE devices [28].

2.1.4. Cobalt Oxide-Based Thin Films

Cobalt oxide-based thin films, like NaCoO_x with two-dimensional layered structure, exhibit high power factor in the in-plane direction [44,45]. An example of NaCo₂O₄ single crystal thin film showed the TE power of 100 μ V K⁻¹ at 300 K [46]. Besides these research, Ca₃Co₄O₉ were found with good performance in thermopower at room temperature recently. The single crystal of Ca₃Co₄O₉ presented resistivity of 10–40 m Ω cm, thermopower of 125 μ V K⁻¹, and power factor of 0.04–0.16 mW m⁻¹ K⁻², respectively [47]. The nanostructured Ca₃Co₄O₉ thin films can reach the high power factor above 1 \times 10⁻⁴ W m⁻¹ K⁻² in a wide temperature range. These films are flexible and bendable without any deterioration of the TE performance [48]. When introducing nanoporous structures into Ca₃Co₄O₉ thin films, the TE performance improved due to the selectively scattering phonons. The porosity of Ca₃Co₄O₉ structures can be controlled, which determined the TE properties of the nanoporous Ca₃Co₄O₉ thin films. The lowest electrical resistivity is around 7 m Ω cm, yielding a power factor of 2.32 \times 10⁻⁴ W m⁻¹ K⁻² near room temperature [49]. Furthermore, these films are transferable from the primary substrates to other arbitrary polymer platforms by simple dry transfer, which opens an opportunity for wearable applications. Additionally, layered calcium cobalt oxides and strontium cobalt oxides, synthesizing from sodium cobalt oxide precursors by ion-exchange reactions, displayed an increased power factor [50–52]. The maximum power factor of layered Ca_{0.33}CoO₂ is 9 \times 10⁻⁴ W m⁻¹ K⁻² at 300 K, which is about 25% higher than that of Ca₃Co₄O₉ [52]. The power factor of layered Sr_{0.29}CoO₂ is 3.5 \times 10⁻⁴ W m⁻¹ K⁻² at 300 K [51]. Power factor is more important than the thermal conductivity for TE power generation for a given ZT value, which is due to tuning power factor does not influence thermo-mechanical stability while lowering thermal conductivity leads to severe thermo-mechanical issues [53]. Thus, for low power applications, achieving high power factor is more practical than reducing thermal conductivity in wearable applications.

2.2. Organic-Based Thin Film TE Materials

Apart from inorganic semiconductors discussed above in TE application, organic polymers, or called semi-metallic polymers, inherently possess a low thermal conductivity, which gives them a significant advantage over conventional TE materials [54–57]. After all, semiconducting polymers are potentially abundant, light-weight, flexible, solution-processable, and low-cost [58]. However, most of the polymers suffer poor efficiency, which requires a suitable doping agent to improve their TE performance. Numerous doped *p*-type semiconducting polymers, such as typical polyacetylene, polyaniline, polypyrrole, polythiophene, and poly(3,4-ethylenedioxythiophene), and some typical *n*-type conductive polymers have been researched for their TE applications [59–63].

2.2.1. Polyacetylene and Polyaniline

Iodine-doped polyacetylene film showed the highest value of electrical conductivity of 1×10^5 S/cm, which was better than that in non-doped polyacetylene film (3×10^3 S/cm) [64]. Other metal chlorides, for example, FeCl₃, MoCl₅, NbCl₅, and ZrCl₄, have been doped with polyacetylene. The electrical conductivity and TE power of these doped polyacetylene films have been measured at different temperatures. The results demonstrated that FeCl₃-doped polyacetylene film exhibited the highest value of electrical conductivity of 3×10^5 S/cm at 220 K [65]. Besides, Bi_{0.5}Sb_{1.5}Te₃ nanoplates embedded polyaniline composites presented highly increased Seebeck coefficient and thus an enhanced power factor from 16.5×10^{-8} to 84.4×10^{-8} W m⁻¹ K⁻² at 400 K [66]. However, the obvious disadvantage of polyacetylene is unstable in the atmosphere.

Searching for more stable conducting polymers, the electrically conductive emeraldine salt form of polyaniline is air stable, which is able to produce in large scale in low-cost [67,68]. The combination film of polyaniline with camphorsulfonic acid (CSA) showed good electrical conductivity between 10 K and 300 K. These thin films exhibit metallic conductivity due to the doping level. Among the different doping level, the 60% doped thin films have the electrical conductivity of 300 S/cm [69]. The multilayered polyaniline film (electrically insulating emeraldine based layers and electrically conducting CSA-doped emeraldine salt layers) even presented the higher ZT at 300 K than that of a bulk film of CSA-doped polyaniline [70].

2.2.2. Polypyrrole and Polythiophene

Polypyrrole, distinguished from above two conductive polymers, shows comparatively higher conductivity (>300 S/cm) at very low temperatures ($T \sim 0$ K). A series of polypyrrole samples from different synthesized methods measured the TE power and conductivity as a function of temperature, including chemically synthesized soluble polypyrrole films, wrinkled polypyrrole films on indium-tin-oxide electrodes, films were grown on nonconducting substrates, and polypyrrole gas sensors with different dopants. It turns out that the highest conductivity of 340 S/cm was obtained for polypyrrole that was doped with PF₆ [71].

High-quality free-standing polythiophene and poly(3-methylthiophene) nanofilms with high tensile strength were investigated. They show a decent TE performance of ZT value of 0.03 at 250 K, which is higher than that of many other conducting polymers [72]. Sun et al. initially claimed that high conducting polymers tend to exhibit conductivity from carriers that are close to the Fermi level (Figure 2c). They fabricated poly(3-hexylthiophene) thin film on Si substrate and characterized the thickness of 100 nm (Figure 2d) [73]. Although the TE performance of this thin film was not particularly high, this work demonstrated a theoretical route for reaching a high Seebeck coefficient.

2.2.3. Poly(3,4-ethylenedioxythiophene)

Poly(3,4-ethylenedioxythiophene) is another extensively studied polymer, especially the combination of poly(3,4-ethylenedioxythiophene) and polystyrenesulfonate (PEDOT:PSS). The mixtures show high electrical conductivity along the casting plane [74]. For example, of 20 μm drop-cast films, the thermal

and electrical in-plane conductivities are, respectively, $1.0 \text{ W m}^{-1} \text{ K}^{-1}$ and 500 S cm^{-1} . The high electrical conductivity leads to a highly anisotropic thermal conductivity of drop-cast dimethylsulfoxide (DMSO)-mixed PEDOT: PSS films. When using DMSO post-treatment instead of DMSO addition in the PEDOT: PSS films, the power factor of the film is 65% increased. The electrical conductivity-improving contributes to this increase while the Seebeck coefficient is in minor change [75]. Besides, there is a significant enhancement of the electrical conductivity of PEDOT: PSS (from 787.99 to $4839.92 \text{ S cm}^{-1}$) and Te-PEDOT:PSS hybrid (from 11.01 to 334.68 S cm^{-1}) by chemical treatment with H_2SO_4 [76].

2.2.4. Other *n*-type Polymers

For *n*-type organic TE materials, poly(nickel-ethylenetetrathiolate) (poly(Ni-ett)) reaches the highest ZT value of 0.3 at room temperature [77]. An example shows that the optical power factor of poly(Ni-ett) synthesized at 0.6 V ($131.6 \mu\text{W m}^{-1} \text{ K}^{-2}$ at 360 K) is higher than that of at 1 or 1.6 V via potentiostatic deposition [78]. Poly(benzobisimidazobenzophenanthroline) (BBL) has demonstrated the electron mobility as high as $0.1 \text{ cm}^2 \text{ V}^{-1} \text{ s}^{-1}$ with the field-effect [79]. It can achieve 2.4 S cm^{-1} in the electrical conductivity [80]. As a new class of promising *n*-type organic TE materials, self-doping perylene diimide (PDI) derivatives has been reported with the power factor of $1.4 \mu\text{W m}^{-1} \text{ K}^{-2}$ [81].

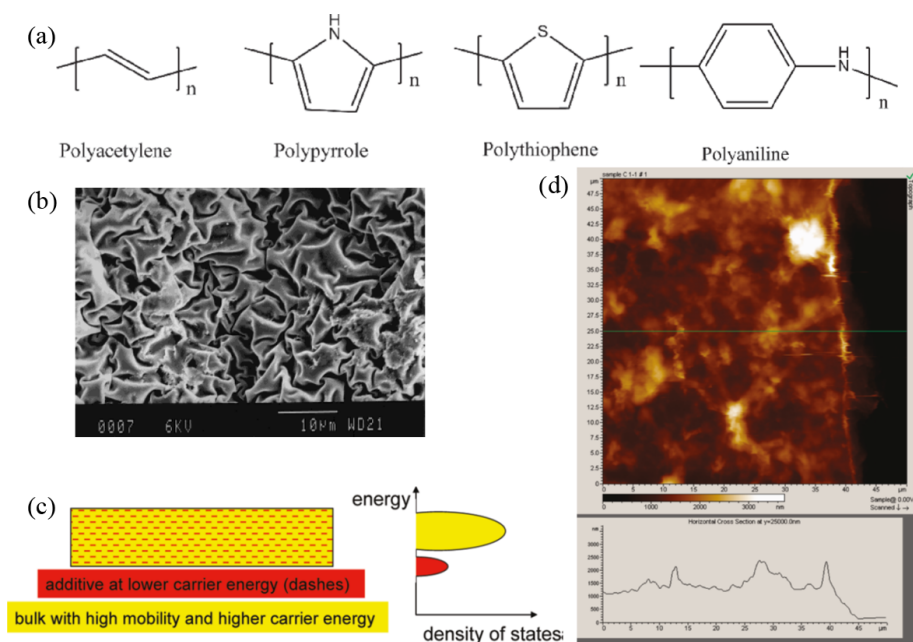


Figure 2. (a) Chemical structures of polyacetylene, polyaniline, polypyrrole, and polythiophene. Reproduced from [61] with permission; Copyright John Wiley & Sons, Inc. 2014; (b) SEM image of the surface of a polypyrrole film (doped with PF_6) that was facing the ITO (indium tin oxide) electrode. Reproduced from [71] with permission; Copyright John Wiley & Sons, Inc. 1999; (c) Schematic illustration of proposed organic TE composite, consisting of an additive that sets the Fermi level and a bulk in which charge carriers at higher energy levels are transported; and (d) Atomic force microscope (AFM) image of drop-cast blend poly(3-hexylthiophene) thin film on Si substrate. Reproduced from [73] with permission; Copyright American Chemical Society 2010.

2.3. Inorganic-Organic Composite Thin Film TE Materials

Although conducting polymer thin films are low density, low cost, low thermal conductivity, and easy synthesis, it has not been feasible to apply these materials along in TE generators due to the limitations of electrical conductivity and ZT value. When combining inorganic materials and organic conducting polymers, both advantages from these two types of materials present significant potential

for producing relatively low-cost and high-performance TE materials [82]. Recently, an increasing number of studies have reported on inorganic-organic thin film TE nanocomposite materials [83].

2.3.1. Metal-Organic Frameworks

Metal-organic frameworks (MOFs) start to be researched in TE application since its electrical conductivity has been reported [84,85]. Recently, the composite of tetracyanoquinodimethane (TCNQ) and $\text{Cu}_3(\text{BTC})_2$ (BTC = benzene tricarboxylate) thin films that are deposited by a solution-based method at room temperature (Figure 3a). The TE properties of these $\text{TCNQ@Cu}_3(\text{BTC})_2$ films were measured under the controlled temperature gradient, which shows the Seebeck coefficient of $375 \mu\text{V/K}$ at room temperature (Figure 3b,c). This value exceeds some organic thin films and even Bi_2Te_3 bulk materials [86]. However, the electrical performance of $\text{TCNQ@Cu}_3(\text{BTC})_2$ film was lower than the above-mentioned TE materials. Although this work presents a new type of TE materials, the TE properties of MOFs films still need to improve.

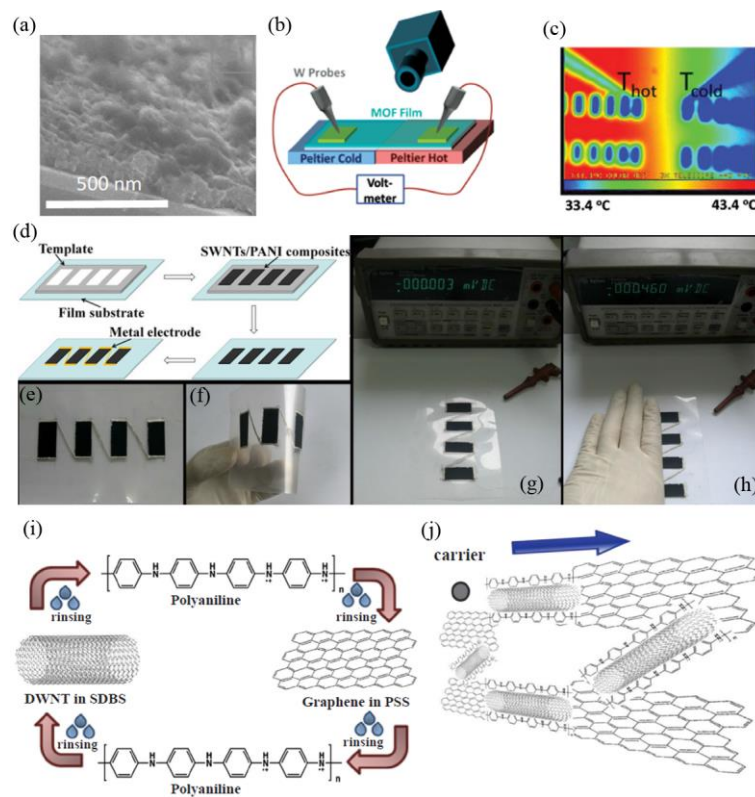


Figure 3. (a) Cross-section SEM image of an infiltrated tetracyanoquinodimethane ($\text{TCNQ@Cu}_3(\text{BTC})_2$) thin film; (b) Schematic illustration of the TE measurement for metal-organic frameworks (MOF) thin film. An infrared (IR) camera is used to measure the temperature difference between heat side and cool side of the substrate and a multimeter is detected for the voltage generated between two of the metal contacts; (c) Example IR image taken during one of the measurements. Reproduced from [86] with permission; Copyright John Wiley & Sons, Inc. 2015; (d) Method for the preparation and assembly of the single-walled carbon nanotubes (SWCNTs)-polyaniline composite thin film TE module; (e,f) Photograph of fabricated flexible TE module; (g,h) Thermal voltage generation from the TE module before and after touching at one side of the module; Reproduced from [87] with permission; Copyright John Wiley & Sons, Inc. 2016; (i) Schematic illustration of the layer-by-layer self-assembly procedure of polyaniline/CNT/graphene multilayer film; and (j) carrier transport in these multilayer film. Reproduced from [88] with permission; Copyright John Wiley & Sons, Inc. 2015.

2.3.2. Carbon Nanotube-Polymer Composites

Carbon nanotubes (CNTs), which are a new star of carbon materials, are increasingly used in TE composites or other energy storage materials due to their remarkable electrical property and low cost [89–94]. A good example is that an excellent flexible *n*-type and *p*-type single-walled CNTs (SWCNTs) networks film showed good power factor of 1.5×10^3 and $1.84 \times 10^3 \mu\text{W m}^{-1} \text{K}^{-2}$, respectively, with a long working lifespan up to three months [25]. A novel technology for decreasing internal resistivity to assemble a flexible TE module based on these CNT films is initially demonstrated, which is different from previous works. Large-area thick *p*-type CNT films were fabricated firstly and then cut into stripes sticking on the substrate. Then, the CNT film stripe was covered alternately for remaining as *p*-type and converted uncovered part into *n*-type. In this technique, the *p*-*n* couples were creatively built in one stripe. Before measuring performance, pasting two metal electrodes for each edge. It is an improving inspiration for the design of flexible TE devices. The SWCNTs-polyaniline composite films were attempted in TE measurement, which presented the power factor was $217 \mu\text{W m}^{-1} \text{K}^{-2}$. In addition, 65 wt % SWCNTs-polyaniline composite segments that were prepared and assembled as a TE module, which can generate $10.4 \mu\text{W m}^{-1} \text{K}^{-2}$ of power efficiency with good stability in the air (Figure 3d–h) [87]. Further research reported that polyaniline/CNT/graphene multilayer film has a comparable power factor of $1.825 \times 10^3 \mu\text{W m}^{-1} \text{K}^{-2}$ at room temperature (Figure 3i,j) [88].

In conclusion, inorganic-based, organic-based, or inorganic-organic composites thin film TE materials present some obvious advantages, including improved power factor, better performance at room temperature, facile synthesis approaches, and low cost of production. Thus, they have great potential in the further development of flexible and portable TE devices.

3. Measurement Technique of Thin Film TE Materials

Different from TE measurements for bulk materials, the accurate characterization of TE performance in thin films is challenging. In 1958, T.C. Harman first published a measurement method, which is called the Harman method, utilized for measuring the ZT value in many works [95]. However, this method is not accurate for applying to thin films due to the slow thermal response of thin films and insensitive of small transient Seebeck voltage [96]. In much research, TE data of thin films were obtained using homemade apparatus for matching samples at different characteristics [97,98]. Thus, there is no uniform measurement method for all kinds of thin film TE materials. Because of that, some novel measurement techniques for electrical conductivity (σ), Seebeck coefficient (S), and thermal conductivity (κ), which will discuss as following, are developed for simple and more accurate characterization for thin films.

3.1. Electrical Conductivity

The electrical conductivity (σ) for thin films was measured with a four-point probe device. Although two-point measurement is generally used for bulk TE materials, the four-point method can eliminate any contact resistance during the measurement when considering the very thin thickness of the films (Figure 4a). Electrical conductivity can be calculated by the following equation:

$$\sigma = 1/\rho \quad (1)$$

$$\rho = (V/l)/[I/(wt)] \quad (2)$$

in which ρ is electrical resistivity, V and I are measured voltage and current, l is the length of electrons travel, and w and t are the width and thickness of a sample. The length (l) is the spacing of the probe tips and the width (w) is estimated by the software. The thickness (t) of each sample was measured with surface profilometry using a KLA Tencor P-16+ [99]. Firstly, three lines were scratched onto the

sample without destroying the surface of the substrate (Figure 4b). Then, the step height was measured at each of these scratches. The thickness of the samples is estimated by the following equation:

$$t = \{[(t_1 + t_3)/2] + t_2\}/2 \quad (3)$$

For more accuracy, several electrical conductivity measurements will be taken near the center of the sample and calculate the average (Figure 4c).

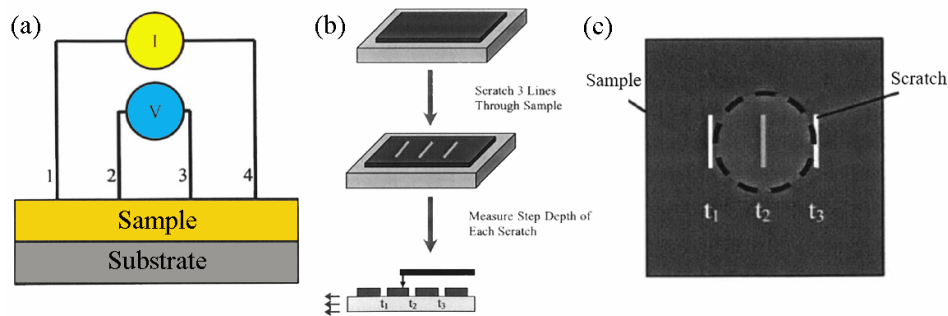


Figure 4. (a) Four-point electrical conductivity circuit. Current is supplied between pin 1 to pin 4, while voltage is measured between pin 2 to pin 3; (b) The process and locations of thickness measurements using the profilometer; and (c) The electrical conductivity measurement area of the sample. Reproduced from [99] with permission; Copyright Massachusetts Institute of Technology 2013.

3.2. Seebeck Coefficient

In Snyder's work, a scanning apparatus is reported to directly detect local variations of Seebeck coefficient on thin film samples. This scanning Seebeck coefficient measurement system is ideal for thin film samples, especially since it can measure films directly without separation from substrates [100]. A typical scanning Seebeck coefficient measurement system has a "hot probe" and a "cold probe", in which they create the temperature gradient for the Seebeck coefficient measurement. In this setup, the heater is located on the sample holder side, and the cold (room-temperature) scanning probe acts as a cold finger. In Figure 5a, one probe keeps the same temperature and is electrically connected to the bottom of the sample surface and the other probe with a thermocouple junction at the tip contact with the film sample surface moving under the motorized stage. A simulated sample test process is shown in Figure 5b. The unique merit of this Seebeck coefficient measurement system is no requirement for substrate removal, which means that the homogeneity of the film sample deposited on an insulating substrate (or multilayer film insulated from a conducting substrate) can be directly evaluated. This merit simplifies the measurement steps and eliminates the possibility of sample degradation. Thus, the thermocouple junction is located onto the same surface where the scanning probe contacts, but at a different temperature determined by the substrate temperature, as shown in Figure 5c,d.

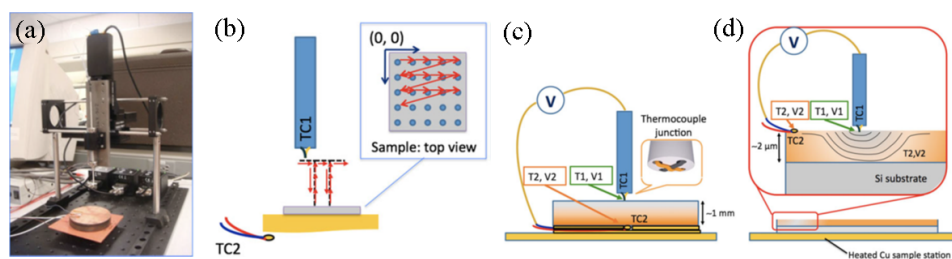


Figure 5. (a) Photograph of the scanning Seebeck coefficient measurement system and (b) schematic illustration of the scanning tip routes; Schematic illustration of the setup for (c) bulk and (d) thin-film samples. Reproduced from [100] with permission; Copyright Springer 2012.

3.3. Thermal Conductivity

The experimental measurement of thermal conductivity (κ) for thin films, to some extent, results in a manifest error ($\sim\pm 10\%$) [101]. Some developed novel solutions can calibrate the experimental error and present fast measurement approaches. For instance, “steady-state isothermal technique” improves accuracy by collecting data under conditions where thermal losses and errors are unimportant. Analysis of this technique while using a Peltier cooler demonstrates the error of less than 1% [102]. When considering real TE generators, including qualitative demonstration, experimental uncertainty is reduced by this technique by more than a factor of 2. “Scanning hot-probe” and “lock-in transient Harman” methods reduce error by highly detailed treatment of interfacial contact effects, including electrical contact resistance and thermal contact effects. In scanning hot-probe technique, average probe temperature is also measured far from the sample to avoid the amount of heat loss. The heat transfer coefficient of “lock-in transient Harman” method was determined to be about 2%. Its uncertainty was assumed to be closer to 10% [103]. In addition, the thermal conductivity along the cross-plane and in-plane direction have been measured and reported by the 3ω methods and time-domain thermoreflectance measurements (TDTR) [26,55,74]. However, these two methods still need to be improved for the measurement of thin films with a relatively large surface roughness [62]. A self-heating 3ω method was used to solve the problem for the in-plane measurement where a gold wire with width should be thinner or comparable to the film thickness. In this method, the self-supported thin film with substrate acted both as a heater to create a temperature fluctuation and a sensor to measure the thermal response under a four-probe resistance measurement configuration (Figure 6a,b) [104].

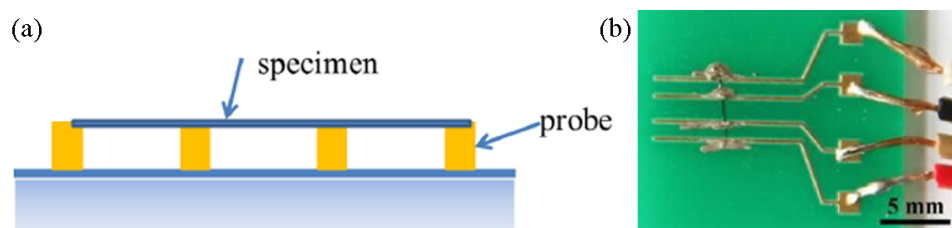


Figure 6. (a) Schematic illustration of the four-probe configuration for measuring the specific heat and thermal conductivity of a filament-like specimen; and (b) The four-probe configuration on the specimen holder for measuring the in-plane thermal conductivity of the film. Reproduced from [62] with permission; Copyright John Wiley & Sons, Inc. 2016.

4. Conclusions and Outlooks

In summary, traditional inorganic TE semi-conductive materials have been restricted, to some extent, in their stagnancy of performance and high cost. Although low-dimensional inorganic TE materials, such as superlattices and thin films, have been proved in decreasing thermal conductivity in many researches, the overall TE performance is insufficient to investigate TE devices. Furthermore, the TE working temperature of inorganic materials is usually above 500 K, which is the fatal weakness of these kind materials in the development of portable and wearable devices. The ideal TE devices are best served at room temperature or low temperature, which makes it easier to meet working temperature requirement.

When compared to inorganic materials, organic conducting polymer thin films have many features, including low cost, facile synthesis, lower working temperature, and low thermal conductivity, and they attract increasing attention. However, these organic polymer TE thin films still need to improve electrical conductivity and Seebeck coefficient in TE measurements.

Recently, the study of the combination of inorganic-organic composite TE materials is a possible strategy to meet breakthrough in intelligent TE devices, especially introducing high-performance

inorganic TE materials into polymer thin films. The hybridization of CNTs or graphene and polymer thin films have been displayed amazing TE performance in many reports. As a recently developed strategy, inorganic-organic composite TE thin films is a promising direction for portable and wearable TE devices in the future, because they can achieve high TE performance, benefiting from both high electrical conductivity of inorganic materials and poor thermal conductivity of organic conducting polymers.

TE measurement technique, especially for thin films, is another hurdle to be conquered in the development of devices. Although it is sufficient that the theoretical fundamentals and experimental techniques of TE measurements in bulk materials, the measurement of thin films cannot rely solely on above theories and experimental techniques. In this case, a series of measurements of TE thin films are using a homemade apparatus for matching characteristics of samples. The accuracy of measured results is the priority of these research. Meantime, the improvement of measurement techniques is an auxiliary means to achieve the better performance of TE devices.

The interest in the development of portable and wearable TE devices will never terminate. As the inspiration of thin film TE materials, a prototype with liquid TE legs is under exploration, which can solve potential damage easily in the usage of TE devices. When compared with solid materials, liquid materials possess attractive advantages consisting of excellent deformability, ease of doping, and self-healing abilities, which could afford great promise for intelligent TE devices.

Funding: This project was funded by the National Natural Science Foundation of China (51702091, 51702046, 51772050, and 51432004), the Natural Science Foundation of Hubei Province, China (2017CFB192), the Innovation Program of Shanghai Municipal Education Commission (2017-01-07-00-03-E00025), the Shanghai Committee of Science and Technology, China (17ZR1401000, 18JC1411200 and 16JC1401800), China Postdoctoral Science Foundation (2017M621320), the Fundamental Research Funds for the Central Universities, the Programme of Introducing Talents of Discipline to Universities (111-2-04), DHU Distinguished Young Professor Program, Shanghai Pujiang Program (17PJ1400100), and State Key Laboratory for Modification of Chemical Fibers and Polymer Materials, Donghua University.

Conflicts of Interest: The authors declare no conflict of interest. The founding sponsors had no role in the design of the study; in the collection, analyses, or interpretation of data; in the writing of the manuscript, and in the decision to publish the results.

References

1. Service, R.F. Temperature rises for devices that turn heat into electricity. *Science* **2004**, *306*, 806–807. [[CrossRef](#)] [[PubMed](#)]
2. Lan, Y.; Minnich, A.J.; Chen, G.; Ren, Z. Enhancement of thermoelectric figure-of-merit by a bulk nanostructuring approach. *Adv. Funct. Mater.* **2010**, *20*, 357–376. [[CrossRef](#)]
3. Nielsch, K.; Bachmann, J.; Kimling, J.; Böttner, H. Thermoelectric nanostructures: From physical model systems towards nanograined composites. *Adv. Energy Mater.* **2011**, *1*, 713–731. [[CrossRef](#)]
4. Yang, J.; Shen, D.; Zhou, L.; Li, W.; Li, X.; Yao, C.; Wang, R.; El-Toni, A.M.; Zhang, F.; Zhao, D. Spatially confined fabrication of core-shell gold nanocages@mesoporous silica for near-infrared controlled photothermal drug release. *Chem. Mater.* **2013**, *25*, 3030–3037. [[CrossRef](#)]
5. Yang, J.; Wang, Y.; Chou, S.; Zhang, R.; Xu, Y.; Fan, J.; Zhang, W.; Liu, H.; Zhao, D.; Dou, S. Yolk-shell silicon-mesoporous carbon anode with compact solid electrolyte interphase film for superior lithium-ion batteries. *Nano Energy* **2015**, *18*, 133–142. [[CrossRef](#)]
6. Yang, J.; Wang, Y.; Li, W.; Wang, L.; Fan, Y.; Jiang, W.; Luo, W.; Wang, Y.; Kong, B.; Selomulya, C.; et al. Amorphous TiO₂ shells: A vital elastic buffering layer on silicon nanoparticles for high-performance and safe lithium storage. *Adv. Mater.* **2017**, *29*, 1700523. [[CrossRef](#)] [[PubMed](#)]
7. Wang, Q.; Zhao, Y.; Luo, W.; Jiang, W.; Fan, J.; Wang, L.; Jiang, W.; Zhang, W.; Yang, J. Iron nanoparticles in capsules: Derived from mesoporous silica-protected prussian blue microcubes as efficient selenium removal. *Chem. Commun.* **2018**, *46*, 5887–5890. [[CrossRef](#)] [[PubMed](#)]
8. Minnich, A.J.; Dresselhaus, M.S.; Ren, Z.; Chen, G. Bulk nanostructured thermoelectric materials: Current research and future prospects. *Energy Environ. Sci.* **2009**, *2*, 466–479. [[CrossRef](#)]

9. Snyder, G.J.; Toberer, E.S. Complex thermoelectric materials. *Nat. Mater.* **2008**, *7*, 105–114. [[CrossRef](#)] [[PubMed](#)]
10. Bell, L.E. Cooling, heating, generating power, and recovering waste heat with thermoelectric systems. *Science* **2008**, *321*, 1457–1461. [[CrossRef](#)] [[PubMed](#)]
11. Wu, Y.; Finefrock, S.W.; Yang, H. Nanostructured thermoelectric: Opportunities and challenges. *Nano Energy* **2012**, *1*, 651–653. [[CrossRef](#)]
12. Vineis, C.J.; Shakouri, A.; Majumdar, A.; Kanatzidis, M.G. Nanostructured thermoelectrics: Big efficiency gains from small features. *Adv. Mater.* **2010**, *22*, 3970–3980. [[CrossRef](#)] [[PubMed](#)]
13. Zhang, G.; Yu, Q.; Wang, W.; Li, X. Nanostructures for thermoelectric applications: Synthesis, growth mechanism, and property studies. *Adv. Mater.* **2010**, *22*, 1959–1962. [[CrossRef](#)] [[PubMed](#)]
14. Seebeck, T.J. Ueber die magnetische polarisation der metalle and erze durch temperatur-differenz. *Ann. Phys.* **1821**, *82*, 133–160. (In Germany) [[CrossRef](#)]
15. Qiu, P.; Shi, X.; Chen, L. Cu-based thermoelectric materials. *Energy Storage Mater.* **2016**, *3*, 85–97. [[CrossRef](#)]
16. Dennler, G.; Chmielowski, R.; Jacob, S.; Capet, F.; Roussel, P.; Zastrow, S.; Nielsch, K.; Opahle, I.; Madsen, G.K.H. Are binary copper sulfides/selenides really new and promising thermoelectric materials? *Adv. Energy Mater.* **2014**, *4*, 1301581. [[CrossRef](#)]
17. Han, C.; Sun, Q.; Li, Z.; Dou, S. Thermoelectric enhancement of different kinds of metal chalcogenides. *Adv. Energy Mater.* **2016**, *6*, 1600498. [[CrossRef](#)]
18. Böttner, H.; Chen, G.; Venkatasubramanian, R. Aspects of thin-film superlattice thermoelectric materials, devices, and applications. *MRS Bull.* **2006**, *31*, 211–217. [[CrossRef](#)]
19. Harman, T.C.; Taylor, P.J.; Walsh, M.P.; LaForge, B.E. Quantum dot superlattice thermoelectric materials and devices. *Science* **2002**, *297*, 2229–2232. [[CrossRef](#)] [[PubMed](#)]
20. Zhao, W.; Liu, Z.; Sun, Z.; Zhang, Q.; Wei, P.; Mu, X.; Zhou, H.; Li, C.; Ma, S.; He, D.; et al. Superparamagnetic enhancement of thermoelectric performance. *Nature* **2017**, *549*, 247–251. [[CrossRef](#)] [[PubMed](#)]
21. Chen, X.; Li, Z.; Dou, S. Ambient facile synthesis of gram-scale copper selenide nanostructures from commercial copper and selenium powder. *ACS Appl. Mater. Interfaces* **2015**, *7*, 13295–13302. [[CrossRef](#)] [[PubMed](#)]
22. Chen, X.; Li, Z.; Yang, J.; Sun, Q.; Dou, S. Aqueous preparation of surfactant-free copper selenide nanowires. *J. Colloid Interface Sci.* **2015**, *442*, 140–146. [[CrossRef](#)] [[PubMed](#)]
23. Zhang, L.; Chen, X.; Han, C. Application prospects of thermoelectric technique. *Res. Dev. Mater. Sci.* **2018**, *3*, 000571.
24. Chen, Z.; Shi, X.; Zhao, L.; Zou, J. High-performance SnSe thermoelectric materials: Progress and future challenge. *Prog. Mater. Sci.* **2018**, *97*, 283–346. [[CrossRef](#)]
25. Zhou, W.; Fan, Q.; Zhang, Q.; Cai, L.; Li, K.; Gu, X.; Yang, F.; Zhang, N.; Wang, Y.; Liu, H.; et al. High-performance and compact-designed flexible thermoelectric modules enabled by a reticulate carbon nanotube architecture. *Nat. Commun.* **2017**, *8*, 14886. [[CrossRef](#)] [[PubMed](#)]
26. Bubnova, O.; Khan, Z.U.; Malti, A.; Braun, S.; Fahlman, M.; Berggren, M.; Crispin, X. Optimization of the thermoelectric figure of merit in the conducting polymer poly(3,4-ethylenedioxythiophene). *Nat. Mater.* **2011**, *10*, 429–433. [[CrossRef](#)] [[PubMed](#)]
27. Lin, Z.; Hollar, C.; Kang, J.; Yin, A.; Wang, Y.; Shiu, H.; Huang, Y.; Hu, Y.; Zhang, Y.; Duan, X. A solution processable high-performance thermoelectric copper selenide thin film. *Adv. Mater.* **2017**, *29*, 1606662. [[CrossRef](#)] [[PubMed](#)]
28. Yang, C.; Souchay, D.; Kneiss, M.; Bogner, M.; Wei, H.; Lorenz, M.; Oeckler, O.; Benstetter, G.; Fu, Y.; Grundmann, M. Transparent flexible thermoelectric material based on non-toxic earth-abundant *p*-type copper iodide thin film. *Nat. Commun.* **2017**, *8*, 16076. [[CrossRef](#)] [[PubMed](#)]
29. Dresselhaus, M.S.; Chen, G.; Tang, M.; Yang, R.; Lee, H.; Wang, D.; Ren, Z.; Fleurial, J.P.; Gogna, P. New directions for low-dimensional thermoelectric materials. *Adv. Mater.* **2007**, *19*, 1043–1053. [[CrossRef](#)]
30. Zhang, Q.; Ai, X.; Wang, L.; Chang, Y.; Luo, W.; Jiang, W.; Chen, L. Improved thermoelectric performance of silver nanoparticles-dispersed Bi₂Te₃ composites deriving from hierarchical two-phased heterostructure. *Adv. Funct. Mater.* **2015**, *25*, 966–976. [[CrossRef](#)]
31. Venkatasubramanian, R.; Siivola, E.; Colpitts, T.; O’Quinn, B. Thin-film thermoelectric devices with high room-temperature figures of merit. *Nature* **2001**, *413*, 597–602. [[CrossRef](#)] [[PubMed](#)]

32. Takashiri, M.; Shirakawa, T.; Miyazaki, K.; Tsukamoto, H. Fabrication and characterization of bismuth-telluride-based alloy thin film thermoelectric generators by flash evaporation method. *Sens. Actuators A-Phys.* **2007**, *138*, 329–334. [[CrossRef](#)]
33. Venkatasubramanian, R.; Colpitts, T.; O'Quinn, B.; Liu, S.; El-Masry, N.; Lamvik, M. Low-temperature organometallic epitaxy and its application to superlattice structures in thermoelectrics. *Appl. Phys. Lett.* **1999**, *75*, 1104–1106. [[CrossRef](#)]
34. Fan, P.; Li, Y.; Zheng, Z.; Lin, Q.; Luo, J.; Liang, G.; Zhang, M.; Chen, M. Thermoelectric properties optimization of Al-doped ZnO thin films prepared by reactive sputtering Zn-Al alloy target. *Appl. Surf. Sci.* **2013**, *284*, 145–149. [[CrossRef](#)]
35. Fan, P.; Zheng, Z.; Li, Y.; Lin, Q.; Luo, J.; Liang, G.; Cai, X.; Zhang, D.; Ye, F. Low-cost flexible thin film thermoelectric generator on zinc based thermoelectric materials. *Appl. Phys. Lett.* **2015**, *106*, 073901. [[CrossRef](#)]
36. Teranishi, T.; Mori, Y.; Hayashi, H.; Kishimoto, A. Thermoelectric property of polycrystalline aluminum-doped zinc oxide enhanced by micropore foaming. *J. Am. Ceram. Soc.* **2012**, *95*, 690–695. [[CrossRef](#)]
37. Ghosh, C.K.; Das, S.; Chattopadhyay, K.K. Enhancement of thermopower of Mn doped ZnO thin film. *Phys. B Condens. Matter* **2007**, *399*, 38–46. [[CrossRef](#)]
38. Loureiro, J.; Neves, N.; Barros, R.; Mateus, T.; Santos, R.; Filonovich, S.; Reparaz, S.; Sotomayor-Torres, C.M.; Wyczisk, F.; Divay, L.; et al. Transparent aluminium zinc oxide thin films with enhanced thermoelectric properties. *J. Mater. Chem. A* **2014**, *2*, 6649–6655. [[CrossRef](#)]
39. Chen, X.; Bai, Y.; Li, Z.; Wang, L.; Dou, S. Ambient synthesis of one-/two-dimensional CuAgSe ternary nanotubes as counter electrodes of quantum-dot-sensitized solar cells. *ChemPlusChem* **2016**, *81*, 414–420. [[CrossRef](#)]
40. Chen, X.; Li, Z.; Bai, Y.; Sun, Q.; Wang, L.; Dou, S. Room-temperature synthesis of Cu_{2-x}E (E = S, Se) nanotubes with hierarchical architecture as high-performance counter electrodes of quantum-dot-sensitized solar cells. *Chem. Eur. J.* **2015**, *21*, 1055–1063. [[CrossRef](#)] [[PubMed](#)]
41. Tan, M.; Chen, X. Growth mechanism of single crystal nanowires of fcc metals (Ag, Cu, Ni) and hcp metal (Co) electrodeposited. *J. Electrochem. Soc.* **2012**, *159*, K15–K20. [[CrossRef](#)]
42. Nunna, R.; Qiu, P.; Yin, M.; Chen, H.; Hanus, R.; Song, Q.; Zhang, T.; Chou, M.; Agne, M.T.; He, J.; et al. Ultrahigh thermoelectric performance in Cu₂Se-based hybrid materials with highly dispersed molecular CNTs. *Energy Environ. Sci.* **2017**, *10*, 1928–1935. [[CrossRef](#)]
43. Yang, C.; Kneiß, M.; Lorenz, M.; Grundmann, M. Room-temperature synthesized copper iodide thin film as degenerate p-type transparent conductor with a boosted figure of merit. *Proc. Natl. Acad. Sci.* **2016**, *113*, 12929–12933. [[CrossRef](#)] [[PubMed](#)]
44. Ohta, H. Thermoelectrics Based on Metal Oxide Thin Films. In *Metal Oxide-Based Thin Film Structures: Formation, Characterization and Application of Interface-Based Phenomena, A Volume in Metal Oxides*; Pryds, N., Esposito, V., Eds.; Elsevier: Amsterdam, The Netherlands, 2018; pp. 441–464.
45. Ravichandran, J. Thermoelectric and thermal transport properties of complex oxide thin films, heterostructures and superlattices. *J. Mater. Res.* **2016**, *32*, 183–203. [[CrossRef](#)]
46. Terasaki, I.; Sasago, Y.; Uchinokura, K. Large thermoelectric power in NaCo₂O₄ single crystals. *Phys. Rev. B* **1997**, *56*, 685–687. [[CrossRef](#)]
47. Masset, A.C.; Michel, C.; Maignan, A.; Hervieu, M.; Toulemonde, O.; Studer, F.; Raveau, B. Misfit-layered cobaltite with an anisotropic giant magnetoresistance Ca₃Co₄O₉. *Phys. Rev. B* **2000**, *62*, 166–175. [[CrossRef](#)]
48. Paul, B.; Lu, J.; Eklund, P. Nanostructural tailoring to induce flexibility in thermoelectric Ca₃Co₄O₉ thin films. *ACS Appl. Mater. Interfaces* **2017**, *9*, 25308–25316. [[CrossRef](#)] [[PubMed](#)]
49. Paul, B.; Bjork, E.M.; Kumar, A.; Lu, J.; Eklund, P. Nanoporous Ca₃Co₄O₉ thin films for transferable thermoelectrics. *ACS Appl. Energy Mater.* **2018**, *1*, 2261–2268. [[CrossRef](#)] [[PubMed](#)]
50. Gushing, B.L.; Falster, A.U.; Simmons, W.B.; Wiley, J.B. A multivalent ion exchange route to lamellar calcium cobalt oxides Ca_xCoO₂ (x ≤ 0.5). *Chem. Commun.* **1996**, *23*, 2635–2636. [[CrossRef](#)]
51. Liu, J.; Huang, X.; Xu, G.; Chen, L. Thermoelectric properties of layered Sr_{0.29}CoO₂ crystals. *J. Alloy. Compd.* **2013**, *576*, 247–249. [[CrossRef](#)]
52. Liu, J.; Huang, X.; Li, F.; Liu, R.; Chen, L. Low-temperature magnetic and thermoelectric properties of layered Ca_{0.33}CoO₂ crystals. *J. Phys. Soc. Jpn.* **2011**, *80*, 074802. [[CrossRef](#)]

53. Liu, W.; Kim, H.; Jie, Q.; Ren, Z. Importance of high power factor in thermoelectric materials for power generation application a perspective. *Scr. Mater.* **2016**, *111*, 3–9. [[CrossRef](#)]
54. Lévesque, I.; Bertrand, P.O.; Blouin, N.; Leclerc, M.; Zecchin, S.; Zotti, G.; Ratcliffe, C.I.; Klug, D.D.; Gao, X.; Gao, F.; et al. Synthesis and thermoelectric properties of polycarbazole, polyindolocarbazole, and polydiindolocarbazole derivatives. *Chem. Mater.* **2007**, *19*, 2128–2138. [[CrossRef](#)]
55. Kim, G.H.; Shao, L.; Zhang, K.; Pipe, K.P. Engineered doping of organic semiconductors for enhanced thermoelectric efficiency. *Nat. Mater.* **2013**, *12*, 719–723. [[CrossRef](#)] [[PubMed](#)]
56. Bubnova, O.; Khan, Z.U.; Wang, H.; Braun, S.; Evans, D.R.; Fabretto, M.; Hojati-Talemi, P.; Dagnelund, D.; Arlin, J.B.; Geerts, Y.H.; et al. Semi-metallic polymers. *Nat. Mater.* **2014**, *13*, 190–194. [[CrossRef](#)] [[PubMed](#)]
57. Kolasinska, E.; Kolasinski, P. A review on electroactive polymers for waste heat recovery. *Materials* **2016**, *9*, 485. [[CrossRef](#)] [[PubMed](#)]
58. Bubnova, O.; Crispin, X. Towards polymer-based organic thermoelectric generators. *Energy Environ. Sci.* **2012**, *5*, 9345–9362. [[CrossRef](#)]
59. Shi, K.; Zhang, F.; Di, C.; Yan, T.; Zou, Y.; Zhou, X.; Zhu, D.; Wang, J.; Pei, J. Toward high performance *n*-type thermoelectric materials by rational modification of BDPPV backbones. *J. Am. Chem. Soc.* **2015**, *137*, 6979–6982. [[CrossRef](#)] [[PubMed](#)]
60. Dubey, N.; Leclerc, M. Conducting polymers: Efficient thermoelectric materials. *J. Polym. Sci. Polym. Phys.* **2011**, *49*, 467–475. [[CrossRef](#)]
61. Zhang, Q.; Sun, Y.; Xu, W.; Zhu, D. Organic thermoelectric materials: Emerging green energy materials converting heat to electricity directly and efficiently. *Adv. Mater.* **2014**, *26*, 6829–6851. [[CrossRef](#)] [[PubMed](#)]
62. Sun, Y.; Qiu, L.; Tang, L.; Geng, H.; Wang, H.; Zhang, F.; Huang, D.; Xu, W.; Yue, P.; Guan, Y.; et al. Flexible *n*-type high-performance thermoelectric thin films of poly(nickel-ethylenetetra-thiolate) prepared by an electrochemical method. *Adv. Mater.* **2016**, *28*, 3351–3358. [[CrossRef](#)] [[PubMed](#)]
63. Xuan, Y.; Liu, X.; Desbief, S.; Leclère, P.; Fahlman, M.; Lazzaroni, R.; Berggren, M.; Cornil, J.; Emin, D.; Crispin, X. Thermoelectric properties of conducting polymers: The case of poly(3-hexylthiophene). *Phys. Rev. B* **2010**, *82*, 115454. [[CrossRef](#)]
64. Zuzok, R.; Kaiser, A.B.; Pukacki, W.; Roth, S. Thermoelectric power and conductivity of iodine-doped “new” polyacetylene. *J. Chem. Phys.* **1991**, *95*, 1270–1275. [[CrossRef](#)]
65. Park, Y.W.; Yoon, C.O.; Na, B.C.; Shirakawa, H.; Akagi, K. Metallic properties of transition metal halides doped polyacetylene: The soliton liquid state. *Synth. Met.* **1991**, *41*, 27–32. [[CrossRef](#)]
66. Guo, C.; Chu, F.; Chen, P.; Zhu, J.; Wang, H.; Wang, L.; Fan, Y.; Jiang, W. Effectively enhanced thermopower in polyaniline/Bi_{0.5}Sb_{1.5}Te₃ nanoplate composites via carrier energy scattering. *J. Mater. Sci.* **2018**, *53*, 6752–6762. [[CrossRef](#)]
67. Li, J.; Tang, X.; Li, H.; Yan, Y.; Zhang, Q. Synthesis and thermoelectric properties of hydrochloric acid-doped polyaniline. *Synth. Met.* **2010**, *160*, 1153–1158. [[CrossRef](#)]
68. Sun, Y.; Wei, Z.; Xu, W.; Zhu, D. A three-in-one improvement in thermoelectric properties of polyaniline brought by nanostructures. *Synth. Met.* **2010**, *160*, 2371–2376. [[CrossRef](#)]
69. Holland, E.R.; Pomfret, S.J.; Adams, P.N.; Abell, L.; Monkman, A.P. Doping dependent transport properties of polyaniline-CSA films. *Synth. Met.* **1997**, *84*, 777–778. [[CrossRef](#)]
70. Tlshima, N. Conductive polymers as a new type of thermoelectric material. *Macromol. Symp.* **2002**, *186*, 81–86. [[CrossRef](#)]
71. Kemp, N.T.; Kaiser, A.B.; Liu, C.; Chapman, B.; Mercier, O.; Carr, A.M.; Trodahl, H.J.; Buckley, R.G.; Partridge, A.C.; Lee, J.; et al. Thermoelectric power and conductivity of different types of polypyrrole. *J. Polym. Sci. Part B Polym. Phys.* **1999**, *37*, 953–960. [[CrossRef](#)]
72. Lu, B.; Liu, C.; Lu, S.; Xu, J.; Jiang, F.; Li, Y.; Zhang, Z. Thermoelectric performances of free-standing polythiophene and poly(3-methylthiophene) nanofilms. *Chin. Phys. Lett.* **2010**, *27*, 057201.
73. Sun, J.; Yeh, M.L.; Jung, B.J.; Zhang, B.; Feser, J.; Majumdar, A.; Katz, H.E. Simultaneous increase in Seebeck coefficient and conductivity in a doped poly(alkylthiophene) blend with defined density of states. *Macromolecules* **2010**, *43*, 2897–2903. [[CrossRef](#)]
74. Liu, J.; Wang, X.; Li, D.; Coates, N.E.; Segalman, R.A.; Cahill, D.G. Thermal conductivity and elastic constants of PEDOT:PSS with high electrical conductivity. *Macromolecules* **2015**, *48*, 585–591. [[CrossRef](#)]

75. Luo, J.; Billep, D.; Waechtler, T.; Otto, T.; Toader, M.; Gordan, O.; Sheremet, E.; Martin, J.; Hietschold, M.; Zahn, D.R.T.; et al. Enhancement of the thermoelectric properties of PEDOT:PSS thin films by post-treatment. *J. Mater. Chem. A* **2013**, *1*, 7576–7583. [[CrossRef](#)]
76. Bae, E.J.; Kang, Y.H.; Jang, K.S.; Cho, S.Y. Enhancement of thermoelectric properties of PEDOT:PSS and tellurium-PEDOT:PSS hybrid composites by simple chemical treatment. *Sci. Rep.* **2016**, *6*, 18805. [[PubMed](#)]
77. Di, C.A.; Xu, W.; Zhu, D.B. Organic thermoelectrics for green energy. *Natl. Sci. Rev.* **2016**, *3*, 269–271. [[CrossRef](#)]
78. Sun, Y.; Zhang, J.; Liu, L.; Qin, Y.; Sun, Y.; Xu, W.; Zhu, D. Optimization of the thermoelectric properties of poly(nickel-ethylenetetra-thiolate) synthesized via potentiostatic deposition. *Sci. China Chem.* **2016**, *59*, 1323–1329. [[CrossRef](#)]
79. Babel, A.; Jenekhe, S.A. High electron mobility in ladder polymer field-effect transistors. *J. Am. Chem. Soc.* **2003**, *125*, 13656–13657. [[CrossRef](#)] [[PubMed](#)]
80. Wang, S.; Sun, H.; Ail, U.; Vagin, M.; Persson, P.O.A.; Andreasen, J.W.; Thiel, W.; Berggren, M.; Crispin, X.; Fazzi, D.; et al. Thermoelectric properties of solution-processed *n*-doped ladder-type conducting polymers. *Adv. Mater.* **2016**, *28*, 10764–10771. [[CrossRef](#)] [[PubMed](#)]
81. Russ, B.; Robb, M.J.; Brunetti, F.G.; Miller, P.L.; Perry, E.E.; Patel, S.N.; Ho, V.; Chang, W.B.; Urban, J.J.; Chabinyk, M.L.; et al. Power factor enhancement in solution-processed organic *n*-type thermoelectrics through molecular design. *Adv. Mater.* **2014**, *26*, 3473–3477. [[CrossRef](#)] [[PubMed](#)]
82. Du, Y.; Shen, S.Z.; Cai, K.F.; Casey, P.S. Research progress on polymer–inorganic thermoelectric nanocomposite materials. *Prog. Polym. Sci.* **2012**, *37*, 820–841. [[CrossRef](#)]
83. Wan, C.; Gu, X.; Dang, F.; Itoh, T.; Wang, Y.; Sasaki, H.; Kondo, M.; Koga, K.; Yabuki, K.; Snyder, G.J.; et al. Flexible *n*-type thermoelectric materials by organic intercalation of layered transition metal dichalcogenide TiS₂. *Nat. Mater.* **2015**, *14*, 622–627. [[CrossRef](#)] [[PubMed](#)]
84. Sun, L.; Miyakai, T.; Seki, S.; Dinca, M. Mn₂(2,5-disulphydrylbenzene-1,4-dicarboxylate): A microporous metal-organic framework with infinite (–Mn–S–)_∞ chains and high intrinsic charge mobility. *J. Am. Chem. Soc.* **2013**, *135*, 8185–8188. [[CrossRef](#)] [[PubMed](#)]
85. Sheberla, D.; Sun, L.; Blood-Forsythe, M.A.; Er, S.; Wade, C.R.; Brozek, C.K.; Aspuru-Guzik, A.; Dinca, M. High electrical conductivity in Ni₃(2,3,6,7,10,11-hexaiminotriphenylene)₂, a semiconducting metal-organic graphene analogue. *J. Am. Chem. Soc.* **2014**, *136*, 8859–8862. [[CrossRef](#)] [[PubMed](#)]
86. Erickson, K.J.; Leonard, F.; Stavila, V.; Foster, M.E.; Spataru, C.D.; Jones, R.E.; Foley, B.M.; Hopkins, P.E.; Allendorf, M.D.; Talin, A.A. Thin film thermoelectric metal-organic framework with high Seebeck coefficient and low thermal conductivity. *Adv. Mater.* **2015**, *27*, 3453–3459. [[CrossRef](#)] [[PubMed](#)]
87. Wang, L.; Yao, Q.; Xiao, J.; Zeng, K.; Qu, S.; Shi, W.; Wang, Q.; Chen, L. Engineered molecular chain ordering in single-walled carbon nanotubes/polyaniline composite films for high-performance organic thermoelectric materials. *Chem. Asian J.* **2016**, *11*, 1804–1810. [[CrossRef](#)] [[PubMed](#)]
88. Cho, C.Y.; Stevens, B.; Hsu, J.H.; Bureau, R.; Hagen, D.A.; Regev, O.; Yu, C.H.; Grunlan, J.C. Completely organic multilayer thin film with thermoelectric power factor rivaling inorganic tellurides. *Adv. Mater.* **2015**, *27*, 2996–3001. [[CrossRef](#)] [[PubMed](#)]
89. Meng, C.; Liu, C.; Fan, S. A promising approach to enhanced thermoelectric properties using carbon nanotube networks. *Adv. Mater.* **2010**, *22*, 535–539. [[CrossRef](#)] [[PubMed](#)]
90. Yao, Q.; Chen, L.; Zhang, W.; Liufu, S.C.; Chen, X. Enhanced thermoelectric performance of single-walled carbon nanotubes/polyaniline hybrid nanocomposites. *ACS Nano* **2010**, *4*, 2445–2451. [[CrossRef](#)] [[PubMed](#)]
91. Luo, W.; Chen, X.; Xia, Y.; Chen, M.; Wang, L.; Wang, Q.; Li, W.; Yang, J. Surface and interface engineering of silicon-based anode materials for lithium-ion batteries. *Adv. Energy Mater.* **2017**, *7*, 1701083. [[CrossRef](#)]
92. Luo, W.; Shen, D.; Zhang, R.; Zhang, B.; Wang, Y.; Dou, S.; Liu, H.; Yang, J. Germanium nanograin decoration on carbon shell: Boosting lithium-storage properties of silicon nanoparticles. *Adv. Funct. Mater.* **2016**, *26*, 7800–7806. [[CrossRef](#)]
93. Luo, W.; Wang, Y.; Chou, S.; Xu, Y.; Li, W.; Kong, B.; Dou, S.; Liu, H.; Yang, J. Critical thickness of phenolic resin-based carbon interfacial layer for improving long cycling stability of silicon nanoparticle anodes. *Nano Energy* **2016**, *27*, 255–264. [[CrossRef](#)]
94. Luo, W.; Wang, Y.; Wang, L.; Jiang, W.; Chou, S.; Dou, S.; Liu, H.; Yang, J. Silicon/mesoporous carbon/crystalline TiO₂ nanoparticles for highly stable lithium storage. *ACS Nano* **2016**, *10*, 10524–10532. [[CrossRef](#)] [[PubMed](#)]

95. Harman, T.C. Special techniques for measurement of thermoelectric properties. *J. Appl. Phys.* **1958**, *29*, 1373–1374. [[CrossRef](#)]
96. Singh, R.; Bian, Z.X.; Shakouri, A.; Zeng, G.H.; Bahk, J.H.; Bowers, J.E.; Zide, J.M.O.; Gossard, A.C. Direct measurement of thin-film thermoelectric figure of merit. *Appl. Phys. Lett.* **2009**, *94*, 212508. [[CrossRef](#)]
97. Suarez, F.; Parekh, D.P.; Ladd, C.; Vashae, D.; Dickey, M.D.; Öztürk, M.C. Flexible thermoelectric generator using bulk legs and liquid metal interconnects for wearable electronics. *Appl. Energy* **2017**, *202*, 736–745. [[CrossRef](#)]
98. Jia, H.; Tao, X.; Wang, Y. Flexible and self-healing thermoelectric converters based on thermosensitive liquids at low temperature gradient. *Adv. Electron. Mater.* **2016**, *2*, 1600136. [[CrossRef](#)]
99. Kuryak, C.A. Nanostructured Thin Film Thermoelectric Composite Materials Using Conductive Polymer PEDOT:PSS. Master's Thesis, Massachusetts Institute of Technology, Cambridge, MA, USA, April 2013.
100. Iwanaga, S.; Snyder, G.J. Scanning Seebeck coefficient measurement system for homogeneity characterization of bulk and thin-film thermoelectric materials. *J. Electron. Mater.* **2012**, *41*, 1667–1674. [[CrossRef](#)]
101. Wang, H.; Porter, W.D.; Böttner, H.; König, J.; Chen, L.D.; Bai, S.Q.; Tritt, T.M.; Mayolet, A.; Senawiratne, J.; Smith, C.; et al. Transport properties of bulk thermoelectrics—An international round-robin study. Part I: Seebeck coefficient and electrical resistivity. *J. Electron. Mater.* **2013**, *42*, 654–664. [[CrossRef](#)]
102. Taylor, P.J.; Maddux, J.R.; Uppal, P.N. Measurement of thermal conductivity using steady-state isothermal conditions and validation by comparison with thermoelectric device performance. *J. Electron. Mater.* **2012**, *41*, 2307–2312. [[CrossRef](#)]
103. Taylor, P.J.; Wilson, A.; Maddux, J.R.; Borca-Tasciuc, T.; Moran, S.P.; Castillo, E.; Borca-Tasciuc, D. Novel measurement methods for thermoelectric power generator materials and devices. In *Thermoelectrics for Power Generation—A Look at Trends in the Technology*; Skipidarov, S., Nikitin, M., Eds.; INTECH: London, UK, 2016; pp. 389–434.
104. Lu, L.; Yi, W.; Zhang, D. 3ω method for specific heat and thermal conductivity measurements. *Rev. Sci. Instrum.* **2001**, *72*, 2996–3003. [[CrossRef](#)]



© 2018 by the authors. Licensee MDPI, Basel, Switzerland. This article is an open access article distributed under the terms and conditions of the Creative Commons Attribution (CC BY) license (<http://creativecommons.org/licenses/by/4.0/>).